Spatially modulated susceptibility in thin film $La_{2-x}Ba_xCuO_4$

Samantha I. Davis,[1] Rahim R. Ullah,[1,*] Carolina Adamo,[2] Christopher A. Watson,[3,4] John R. Kirtley,[2] Malcolm R. Beasley,[2] Steven A. Kivelson,[1,4] and Kathryn A. Moler[1,2,3,4]

[1]*Department of Physics, Stanford University, Stanford, California 94305, USA*

[2]*Geballe Laboratory for Advanced Materials, Stanford University, Stanford, California 94305, USA*

[3]*Department of Applied Physics, Stanford University, Stanford, California 94305, USA*

[4]*Stanford Institute for Materials and Energy Sciences, SLAC National Accelerator Laboratory, 2575 Sand Hill Road, Menlo Park, California 94025, USA*

(Received 6 April 2018; revised manuscript received 22 June 2018; published 11 July 2018)

The high critical temperature superconductor lanthanum barium copper oxide ($La_{2-x}Ba_xCuO_4$) exhibits a strong anomaly in critical temperature at 1/8th doping, nematicity, and other interesting properties. We report here scanning superconducting quantum interference device imaging of the magnetic fields and susceptibility in a number of thin film $La_{2-x}Ba_xCuO_4$ samples with doping in the vicinity of the 1/8th anomaly. Spatially resolved measurements of the critical temperatures of these samples do not show a pronounced depression at 1/8th doping. They do, however, exhibit strong, nearly linear modulations of the susceptibility ("striae") of multiple samples with surprisingly long periods of 1–4 μm. Counterintuitively, vortices trap in positions of largest diamagnetic susceptibility in these striae. Given the rich interplay of different orders in this material system and its known sensitivity to epitaxial strain, we propose phase separation as a possible origin of these features and discuss scenarios in which that might arise.

DOI: 10.1103/PhysRevB.98.014506

I. INTRODUCTION

Since the discovery of high temperature superconductivity in lanthanum barium copper oxide compounds (LBCO) in 1986 [1], the cuprate perovskites and other unconventional superconductors have attracted enormous interest, not only because of their technological promise but also as a laboratory for exploring concepts in condensed matter physics. Although much progress has been made in understanding high temperature superconductivity [2–4], further development demands the empirical exploration of the properties of these materials.

Here, we have probed the phase diagram of thin film $La_{2-x}Ba_xCuO_4$ over a nominal doping range of $x_{nom} = 0.090$ to $x_{nom} = 0.135$. $La_{2-x}Ba_xCuO_4$ is a system of unconventional superconductors that exhibit d-wave superconductivity [2] at temperatures up to 35 K [1]. Along with other unconventional properties, this renders the standard Bardeen-Cooper-Schrieffer theory insufficient to explain the underlying physics and emergent phenomena of such materials. In particular, a proper account of phenomena such as nematicity [5], pair density wave (PDW) stripes [6], and the one-eighth anomaly [7] pose challenges to current theories of superconductivity. Here we studied six samples of thin film LBCO with thicknesses of approximately 20 nm (see Table I), which were grown on a nearly lattice matched substrate. We used scanning scanning superconducting quantum interference device (SQUID) microscopy [8] to measure the magnetic fields and susceptibilities of the samples over a range of temperatures. We observed striking oscillations ("striae") in the superconducting susceptibility and correlated the behaviors of these striae with other properties of the films.

II. EXPERIMENTAL METHODS

Our microscope implements a dc SQUID (see Fig. 1) with small pickup loops integrated into the body of the SQUID through well-shielded coaxial superconducting leads, allowing for high spatial resolution magnetometry measurements [10]. The addition of a field coil, which is geometrically arranged on the SQUID chip such that it applies a controlled amount of magnetic flux to the sample but zero net flux to the SQUID, allows us to also simultaneously measure the sample's magnetic response to an applied magnetic field, i.e., its magnetic susceptibility [11].

To explore the local superconducting properties of thin film LBCO, we used a SQUID with a 0.1 μm inner and 0.3 μm outer pickup loop radius, and inner and outer field coil radii of 0.5 μm and 1.0 μm, respectively [12]. This enabled us to spatially resolve the diamagnetism of our samples with submicron spatial resolution, thus resolving the micron-scale oscillations in the susceptibility of our samples.

The thin films of $La_{2-x}Ba_xCuO_4$ were grown using shuttered layer-by-layer [13] deposition on 0.1° miscut (100) $LaSrAlO_4$ single crystal substrates in a reactive GENxplor VEECO molecular-beam epitaxy system. A substrate temperature of 750 °C and an oxygen plasma background partial pressure of 2×10^{-6} Torr, which was kept constant until the temperature of the substrate dropped below 150 °C, were used. Ba was evaporated using a low temperature effusion cell, and Cu and La were evaporated using high temperature effusion cells. The flux of each element was measured by a quartz

*Present address: Department of Physics, University of California, Davis, 1 Shields Ave, Davis, California 95616, USA.

TABLE I. Sample parameters. Listed are the sample names, nominal dopings x_{nom}, superconducting critical temperatures T_c, the effective field coil radius R divided by the Pearl length Λ measured at 6 K, and striae period.

Sample	x_{nom}	$T_c(K)$	$R/\Lambda(6K)$	Period (μm)
AC 201	0.090	22.9 ± 1.1	0.02 ± 0.005	2.6–2.7
AC 202	0.098	<5	–	–
AC 173	0.115	23.7 ± 0.2	0.24 ± 0.01	3.4–3.8
AC 174	0.125	29.2 ± 0.2	0.26 ± 0.01	1.0–2.6
AC 200	0.125	29.7 ± 1.4	0.02 ± 0.005	–
AC 175	0.135	27.8 ± 0.3	0.16 ± 0.01	1.2

crystal monitor before the growth, and these measurements were used to determine the nominal doping. Attempts to confirm the doping with x-ray photoemission spectroscopy (XPS) led to inconsistent values, possibly due to the difficulty of making XPS measurements on such thin films. Reflection high-energy electron diffraction (RHEED) [13] was used to monitor both the phase purity and the stoichiometry during film growth. RHEED oscillations taken during fabrication of the films indicate that the samples have a smooth surface. Atomic force microscopy (AFM) measurements (see Fig. 2) reveal that the samples are flat except for 20-nm-thick bumps dispersed over the surface. Similarly sized particles, reported to be SrO of 10–50 nm size, have been reported for annealed $SrLaAlO_4$ (001) surfaces [14]. The placement of the particles is random (see Fig. 2) and so it seems unlikely that they are related to our striae. Although terrace widths comparable to our striae periods are observed in $SrLaAlO_4$ substrates [14], they are not seen in our AFM images. The measured samples are shown in Table I.

We used a liquid helium scanning SQUID microscope system to image the magnetic fields and susceptibilities at different locations on our samples [15]. This microscope allowed us to vary the sample temperature over a wide range while keeping the SQUID sensor superconducting [16].

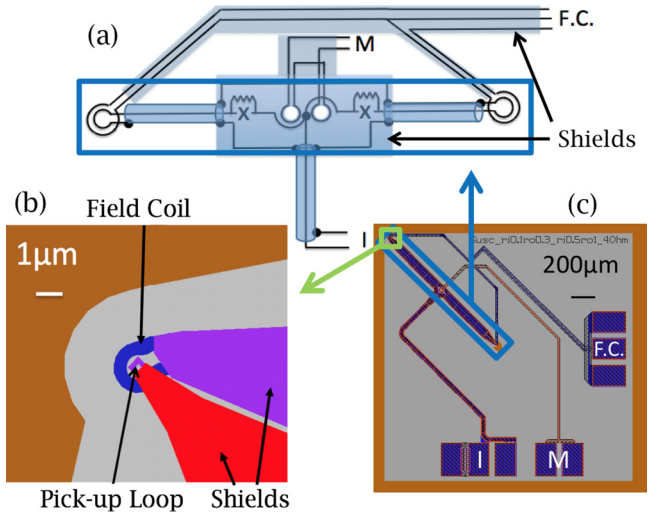

FIG. 1. SQUID Susceptometer with 0.1 μm radius pickup loop. (a) Schematic layout. The current leads, modulation coil, and field coil are labeled by I, M, and $F.C.$, respectively. All but the pickup loop/field coil regions are shielded from external magnetic fields by superconducting layers. (b) Layout of the pickup loop (purple), field coil (blue), and shields (red and purple) region. (c) Layout of the entire 2 mm×2 mm chip.

III. RESULTS

A. Pearl length

We determined the local Pearl length and critical temperature of a sample by moving it toward the SQUID using a z-piezo scanner until contact was reached while measuring the SQUID susceptibility. An example for sample AC174 (see Table I) is shown in Fig. 3. Here a 1 mA, 928 Hz ac current was passed through the field coil. The resultant in-phase flux signal $\phi = \Phi/I$, where Φ is the flux through the SQUID and I is the current through the field coil, was phase sensitively detected and plotted vs the z-piezo scanner voltage as the dots in Fig. 3. The solid lines in Fig. 3 are fits to the data using an expression appropriate for a homogeneous thin film diamagnet [9]:

$$\phi(z) = \phi_{offset} + \alpha(z - z_0) - \phi_s(R/\Lambda)(1 - 2\bar{z}/\sqrt{1 + 4\bar{z}^2}), \quad (1)$$

where $z = c_1 V_z + c_2 V_z^2$, with V_z the piezo voltage, ϕ_{offset} is a constant offset in the susceptibility, due to, e.g., a mismatch in the mutual inductance between the two pairs of field coils/pickup loops, α is a coefficient of a small linear slope in the approach curves, z_0 is the position of the sample when it is in direct mechanical contact with the SQUID substrate, ϕ_s is the mutual inductance between one field coil and one pickup loop, R is the effective radius of the field coil, Λ is the Pearl length of the thin film, and $\bar{z} = (z_0 + \delta_z - z)/R$, where δ_z is the physical spacing between the sample surface and the plane of the pickup loop when the sample and SQUID surface are in contact [9]. We estimate that $\delta z = 0.5 \pm 0.15\,\mu$m. $c_1 = 0.11\,\mu m/V$ was calibrated by measuring a known step height

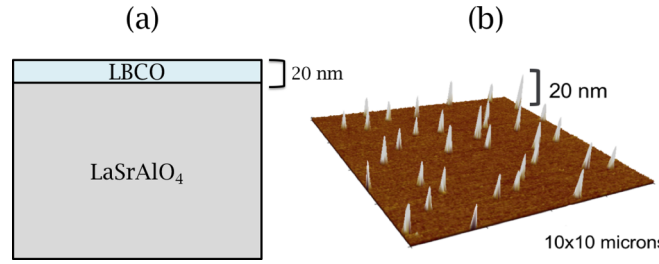

FIG. 2. Sample geometry. (a) Schematic of 20-nm-thick LBCO film on a $LaSrAlO_4$ substrate. (b) AFM image of AC 174, a 20-nm-thick film of $La_xBa_{2-x}CuO_4$ with nominal doping of $x_{nom} = 0.125$.

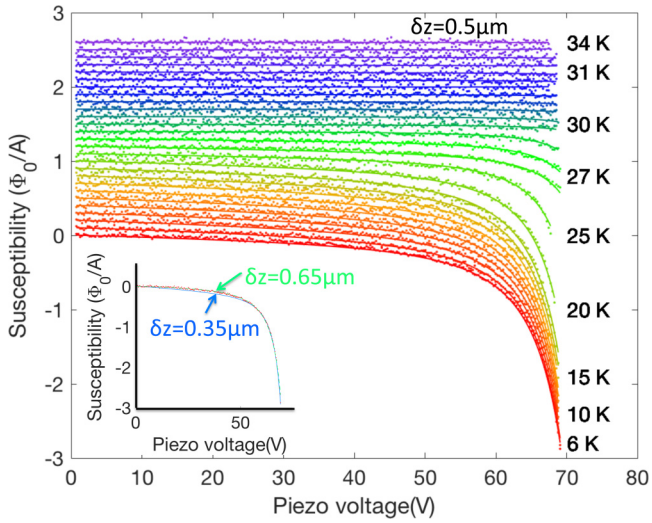

FIG. 3. Susceptibility touchdowns vs temperature. Measurements of the change in the mutual inductance $\phi = \Phi/I$ (in units of $\Phi_0 = h/2e$) between the field coil and the pickup loop in our SQUID susceptometers for sample AC 174 as a function of the z-piezo voltage. The sample comes into mechanical contact with the SQUID substrate at a z-piezo voltage of $V_z = 70$ V. The dots are data, with selective temperatures labeled. The solid lines are fits to Eq. (1). For these fits, we took the measured value $\phi_s = 54\Phi_0/\mathrm{A}$, the effective field coil radius $R = 0.79\,\mu$m [12], the spacing $\delta z = 0.5\,\mu$m, with ϕ_{offset}, c_2, α and R/Λ as fitting parameters. The inset replots the 6 K data, with best fits for δz $= 0.35\,\mu$m (blue solid line) and $0.65\,\mu$m (green dashed line).

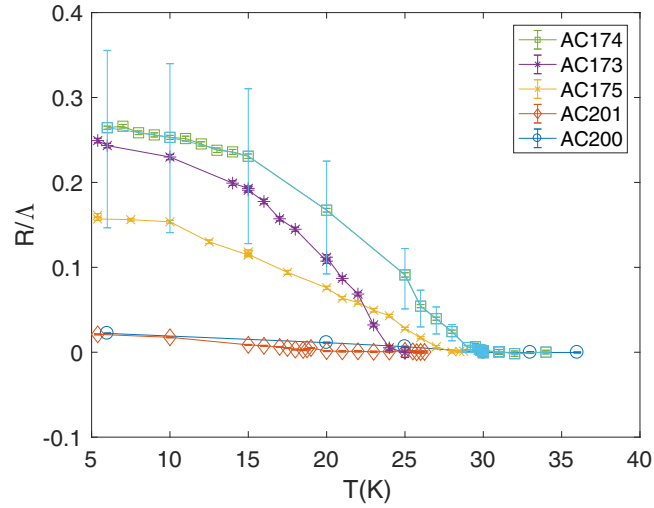

FIG. 4. Pearl length vs temperature. The symbols are fit values for R/Λ from touchdown data as illustrated in Fig. 3, assuming the sample surface to pickup loop distance at contact $\delta z = 0.50\,\mu$m. The error bars on the data for AC174 represent systematic errors due to uncertainty in δz, with the lower and upper bars corresponding to δz $= 0.35\,\mu$m and $0.65\,\mu$m, respectively.

in topographic feedback mode. The small quadratic z-piezo term $c_2 = -1.1\times10^{-4}\,\mu\mathrm{m}/V^2$ was used as a global fitting parameter. The solid lines in the main panel in Fig. 3 are fits assuming $\delta z = 0.5\,\mu$m. The inset of Fig. 3 shows how the fit quality changes when δz is varied between $0.35\,\mu$m and $0.65\,\mu$m. Supplemental Figs. S1-S5 [17] display touchdown data, fits, and the differences between data and fit for the five samples which showed diamagnetic shielding. The theory used here [9] models the pickup loop and field coil as circular wires. There are systematic differences between the fits and data which could presumably be reduced using a more sophisticated model for the field coil/pickup loop region [12]. However, as can be seen in Fig. 4, the largest source of error in these measurements is due to our uncertainty in the spacing between the sample surface and the pickup loop at contact δz: These measurements are most useful for determining either the relative superfluid densities as a function of temperature or sample, or the critical temperatures, but are less precise than could be desired for determining the absolute values of the superfluid density.

The fitting parameters R/Λ for the five samples which showed measurable diamagnetic shielding at 5 K are plotted as the symbols in Fig. 4. Estimates for $R/\Lambda(T = 6\,\mathrm{K})$ and T_c are in Table I. Since for a homogeneous thin film and in the absence of fluctuations the Pearl length $\Lambda = 2\lambda^2/d$, where λ is the London penetration depth and d is the film thickness, and the superfluid density n_s is given by $n_s = m/\mu_0 q^2\lambda^2$, where m is the mass and q is the charge of the superconducting charge carriers, it follows that $n_s(0)/n_s(T) = \Lambda(T)/\Lambda(0)$, and the fitting parameter $R/\Lambda(T)$ is a measure of the superfluid density $n_s(T)$.

An initially surprising result is that, although the low temperature Pearl length varies significantly from sample to sample, the measured critical temperatures of our samples do not, even though their nominal dopings span the $x_{\mathrm{nom}} = 1/8$ range where a sharp drop in critical temperature is observed in bulk LBCO samples. Previous critical temperature measurements on thin film LBCO samples grown on LSAO similarly did not show a 1/8th doping anomaly [18].

B. Striae in susceptibility

Our susceptibility imaging results are also surprising: We find periodic striae of modulated diamagnetism in the susceptibility images of multiple samples. Examples for the five samples with observable diamagnetic susceptibility at 4 K are displayed in Fig. 5. These striae are modulations of the SQUID susceptibility with amplitudes of 1–8% of the total susceptibility and periods from 1–4 μm. These striae did not change in amplitude or period when we changed the scan direction or scan speed. In the four samples in which they are observed, they are seen in all regions of the samples imaged, but with varying orientations, periods, and amplitudes. Individual striae appear to be continuous over distances of at least 81 μm [see, e.g., Fig. 5(d)]. The striae persist, with little variation in period, as the temperature is increased, up to close to the critical temperature. An example is shown in Fig. 6. In this figure simultaneously taken magnetometry images are in the left column, and susceptibility images are in the right column. The data were taken by cooling in a field of $46\,\mu$T, then imaged at successively higher temperatures as labeled. The dashed lines in the susceptibility images show the positions of cross-sections displayed in Fig. 7(a).

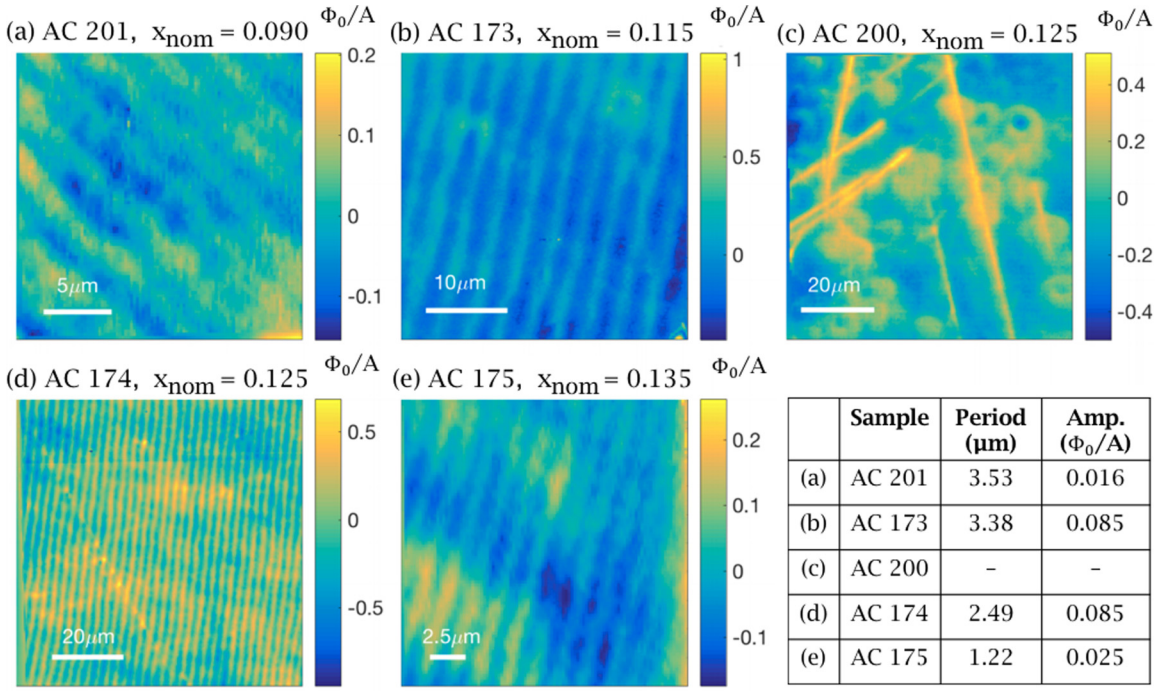

	Sample	Period (μm)	Amp. (Φ_0/A)
(a)	AC 201	3.53	0.016
(b)	AC 173	3.38	0.085
(c)	AC 200	-	-
(d)	AC 174	2.49	0.085
(e)	AC 175	1.22	0.025

FIG. 5. Striae are observed in four of the five superconducting samples imaged. Magnetic susceptibility images of thin-film LBCO for distinct samples with nominal dopings of $0.090 < x_{nom} < 0.135$. The "striae" are the periodic modulations in susceptibility shown in (a), (b), (d), and (e). Note the different scale bars: Striae periods between one and four microns were observed in these samples. An average background susceptibility was subtracted from each of these images. The amplitudes of the striae are approximately 1%, 8%, 4%, and 1% of the total susceptibility of scans (a), (b), (d), and (e), respectively.

Cross-sections through the data of Fig. 6, displayed in Fig. 7(a), show that although there are large, temperature dependent background features in the susceptibility, and the amplitude of the striae fall off as T_c is approached, there is little dependence of the striae periods with temperature. In an effort to better quantify the temperature dependence, we performed two-dimensional Fourier transforms of our susceptibility images. As demonstrated in Fig. 7(b), these transformed images display sharp peaks corresponding to the striae. Figure 7(c) plots the amplitudes and Fig. 7(d) plots the periods of these peaks as a function of temperature. A comparison with the temperature dependence of the Pearl lengths displayed in Fig. 4 shows that the striae amplitudes and periods are less sensitive to temperature than the Pearl lengths.

Although the striae periods depend weakly on temperature, there is a strong relation between striae period and low temperature Pearl length. In sample AC 174 (nominal $x_{nom} = 0.125$) the critical temperature, striae period, and low temperature Pearl length all vary from position to position on the sample. An example is displayed in Fig. 8. Figure 8(a) plots the Pearl lengths at two positions separated by 1 mm. Figure 8(b) plots the stripe period vs $R/\Lambda(T = 5K)$ fit values for four positions, covering a range of 0.7 mm on the sample. This figure shows that there is a nearly linear relation between the stripe period and the low temperature inverse Pearl length. This is at first surprising, since the temperature dependent measurements of, e.g., Fig. 7, show little dependence of the stripe period on temperature, while our touchdown data, e.g., Fig. 4 shows that the Pearl length varies strongly with temperature. This may imply that whatever controls the period, e.g., strain, also modulates the carrier density.

A final clue to the mechanism for striae formation in these samples is their orientation. We found that the stripes do not necessarily align with the crystalline axes, the orientations of the striae vary smoothly from position to position on the sample, and we have never observed boundaries between striae with different orientations.

C. Vortex trapping

Another surprising result is that simultaneous magnetometry and susceptibility images show that superconducting vortices trap on local maxima of the diamagnetic susceptibility. An example of this is shown in Fig. 9. The white dots in the magnetometry image in this figure are superconducting vortices trapped when the sample AC 174 (nominal $x_{nom} = 0.125$) is cooled in a field of approximately 23 μT. The vortex images are elongated by the point spread function of the susceptometer used [9]. Superimposed on the false-color susceptibility images are contour plots of the magnetometry data, which show that the peaks in the vortex magnetic fields line up with the most diamagnetic regions in the susceptibility images.

This striking effect occurs independently of the cooling field used. An example is shown in Fig. 10. In this figure, the left column shows magnetometry data, and the right column shows susceptibility data. Each row in this figure corresponds to simultaneously acquired data, taken after the sample is cooled in fields as labeled. The centers of the vortices are labeled with white dots in both the magnetometry images and the susceptibility images, showing that the vortices are trapped

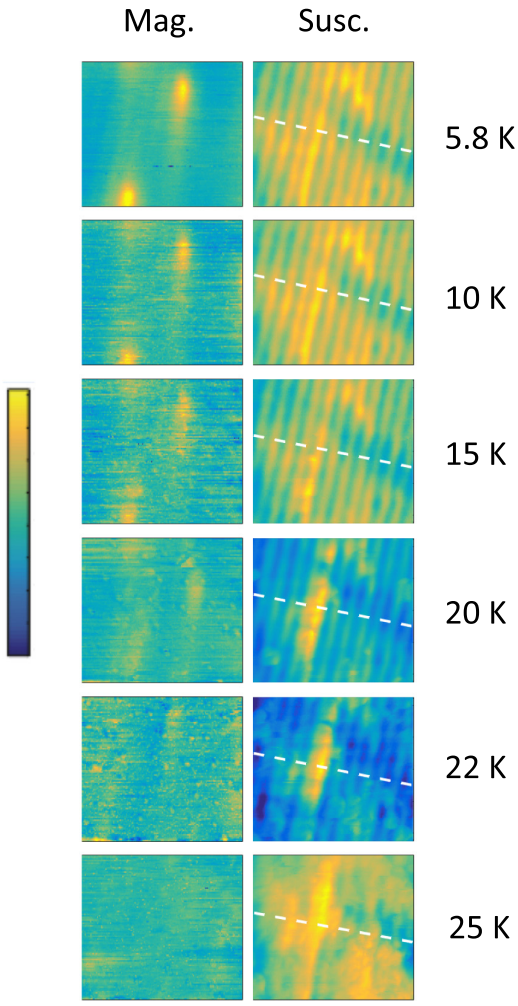

FIG. 6. Striae persist, with little change in period, to close to T_c. Magnetometry (left column) and susceptibility (right column) images of a 10 μm wide by 9 μm high area of sample AC174, cooled and imaged in a field of 33 μT at the temperatures labeled, with a field coil modulation of 10 mA at 2.204 kHz. The false color variations are 4 mΦ_0 for the magnetometry images, and 0.4 Φ_0/A for the susceptibility images. The white dashed lines represent the cross-sections through the data displayed in Fig. 7.

where the diamagnetic susceptibility is largest, for fields from zero up to 1 000 μT.

IV. DISCUSSION

We report here stripelike modulations (striae) in the susceptibility of four samples (out of five measured) of thin film $La_{2-x}Ba_xCuO_4$ with nominal dopings of $0.090 < x_{nom} < 0.135$. The amplitude of the observed modulations of the striae are up to eight percent of the full scale. Due to the point spread function of the pickup loop, the observed amplitude is a lower bound. The periods of the striae range between one and four microns, approximately a thousand times larger than the periods of stripe phases such as the spin and charge density waves that have been measured in bulk samples using neutron and x-ray diffraction techniques [19–21], but comparable to the Pearl lengths in our films. Strikingly, we found that magnetic

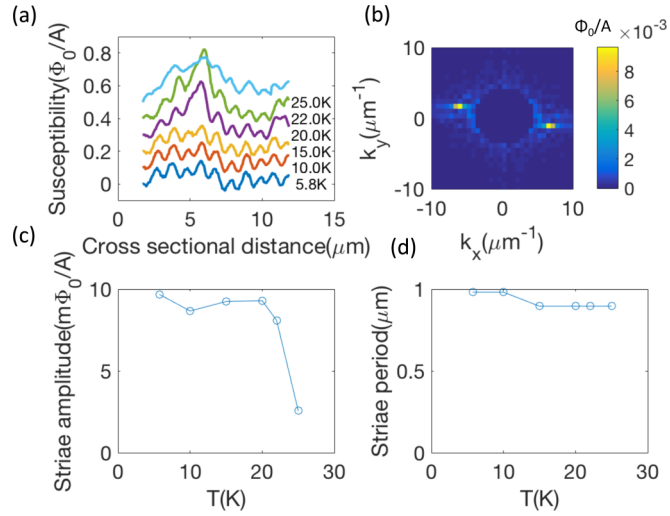

FIG. 7. Temperature dependence of the striae. (a) Cross-sections through the susceptibility data of Fig. 6 at the temperatures labeled. (b) Two-dimensional Fourier transform of the 5.8 K data: the sharp peaks represent the susceptibility striae, with 1 μm period, amplitude $10\,m\Phi_0$/A, and angle of -0.22 radians. (c) Plot of the stripe amplitude, from such Fourier transforms as in (b), as a function of temperature T. (d) Plot of the stripe period vs T.

vortices tend to pin on the diamagnetic maxima of the striae, rather than the minima. The orientation of the striae relative to the crystal axes vary from sample to sample, and from position to position in the same sample.

What causes the striae? They could be simply caused by modulations in film thicknesses d, which would cause oscillations in our observed Pearl lengths Λ through the relation $\Lambda = 2\lambda^2/d$. However, room temperature AFM measurements [Fig. 2(b)] show that the films are flat on the nm scale aside from randomly scattered 20-nm-high bumps. On the other hand, there is a phase transition between room temperature and our measurement temperatures, so buckling is possible. Even so, an oscillation in film thickness would not be expected to cause the vortices to trap on maxima of the diamagnetic susceptibility. Experiments with intentionally introduced thickness variations in aluminum films [22] have been interpreted in terms of pinning on the thin (less diamagnetic) regions [23].

Stripelike patterns have been observed in many systems, such as materials that undergo martensitic phase transitions and thin film type I superconductors. Martensitic phase transi-

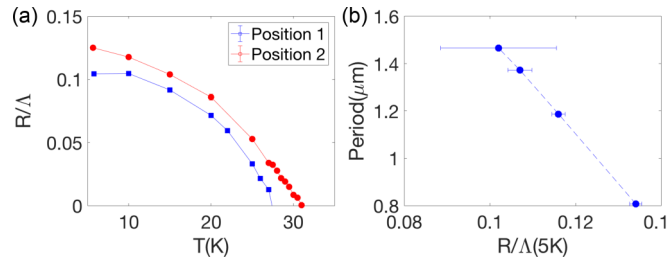

FIG. 8. Stripe period varies with low temperature Pearl length. (a) Fit values from susceptibility touchdown curves for AC174 at two positions separated by 1 mm. (b) Plot of striae period vs fit values for $R/\Lambda(5K)$ at several positions in sample AC174. The dots are data and the dashed lines connect the dots.

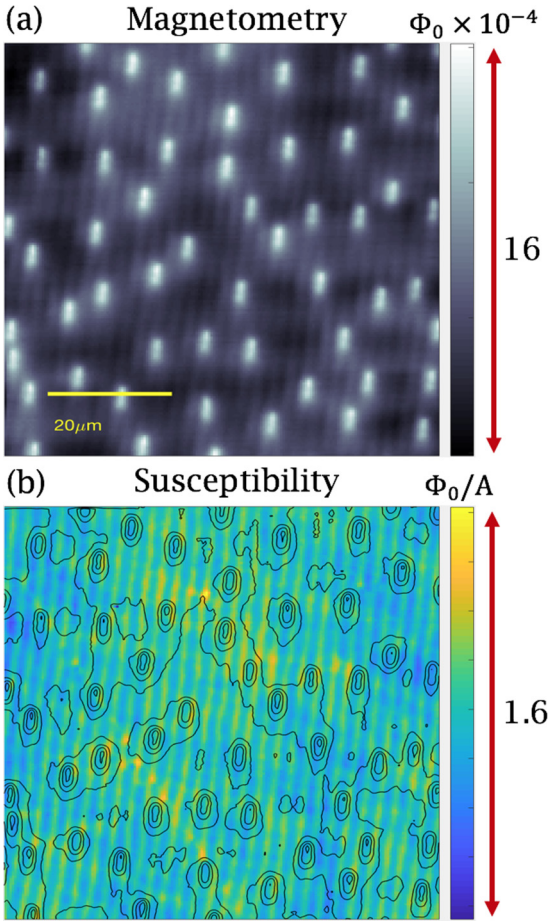

FIG. 9. Superconducting vortices trap at positions of largest diamagnetic susceptibility. Simultaneously acquired magnetometry (upper) and susceptibility (lower) images of sample AC 174, cooled in a field of 23 μT and imaged in field at 5 K. Superposed on the susceptibility image are five equally spaced contours of magnetic flux (in black).

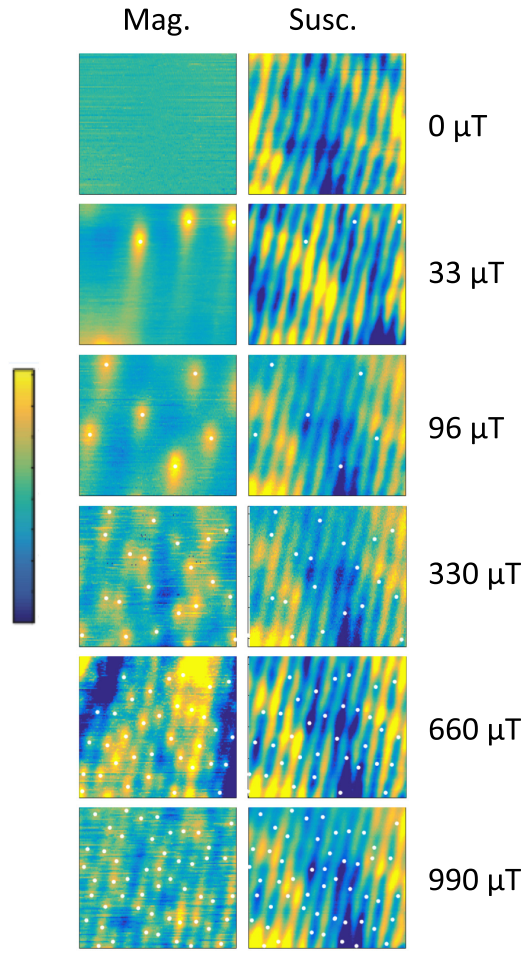

FIG. 10. Vortices trap in regions of largest diamagnetic susceptibility, independent of cooling field. Magnetometry (left column) and susceptibility (right column) images of a 10 μm wide by 9 μm high area of sample AC 174, imaged at $T = 5$ K with a field coil modulation of 10 mA at 2.204 kHz. The samples were cooled and imaged in the fields as labeled. The false color scales are 3 mΦ_0 for the magnetometry images, and 0.1 Φ_0/A for the susceptibility images. The white dots represent the centers of the vortices, offset by -0.25 μm in the susceptibility images to compensate for the displacement between the maximum magnetometry and susceptibility sensitivities for our SQUID sensor.

tions are diffusionless structural transformations of crystalline materials into highly strained lattice structures. Structural changes result from homogeneous lattice deformations, which are commonly driven by quenching or applied stress [24]. To minimize the net strain over large length scales, martensites form elaborate morphologies, such as tweed microstructures, which have domains of unilateral strain along distinct crystal axes [25]. Tetragonal tweed phases have been observed in cuprate superconductors such as yttrium barium copper oxide single crystals [26]. Since experiments have shown that epitaxial strain can enhance local superconductivity in cuprates [27], periodic, stripelike domains of uniaxial strain in a martensite may induce modulations in the Pearl length.

Our observation that the vortices pin in the regions where the diamagnetic susceptibility is higher is surprising, based on numerous previous studies on the pinning of superconducting vortices, particularly in cuprate superconductors. One possibility is that the pinning strength is significantly higher in regions with higher diamagnetic susceptibility. A second is that the vortex self-energy is lower in these regions. The first possibility would require selective pinning in the high pinning strength regions during cooling. While not dismissing this first possibility, we explore the implications of the second.

In general, the total energy of the vortex is the energy in the superfluid and magnetic fields, plus the energy of the core [28]. The superfluid and magnetic energy must be higher in a region with higher diamagnetism [29,30], and generally one would also expect the core energy to be higher in a region with higher diamagnetism. Since we expect that vortices would be attracted to lower energy regions, our observations may imply that the vortex core energy is smaller where the superfluid density is higher.

In most simple theories, one would expect that the core energy is equal to the amount of condensation energy lost in the core, and thus will generally be larger when the superconducting order is stronger. Thus, one needs some more complex situation to make the converse true.

A competing ordered phase that appears in the vortex core would recover some of the condensation energy. Moreover, it is possible that this competing phase is stronger where the superconducting order is stronger, and so causes the vortex core energy to be smaller in such regions. Nothing in the current experiment is sensitive to the precise nature of such a competing phase. Pair density waves (PDW) [6] may be a good candidate, for two reasons: (1) There is new data [31] that suggest that PDW order arises in vortex cores in barium strontium calcium copper oxide. (2) Given that the vortex cores in the cuprates are so small, a competing order in the vortex core must have a condensation energy very close to that of the (dominant) superconducting (SC) state. Since PDW order looks locally much like the uniform superconducting order, it is plausible that it might be very nearly competitive with uniform SC order without fine tuning, and that PDW ordering tendencies could be stronger in precisely the same regions in which SC order is stronger.

Further work to distinguish between these various possibilities would be to measure the dependence of the striae on film thickness and substrate, and to perform vortex dragging experiments [32] to determine the relative pinning strengths of vortices on and off diamagnetic maxima in the striae.

ACKNOWLEDGMENTS

This work was primarily supported by the Department of Energy, Office of Basic Energy Sciences, Division of Materials Sciences and Engineering, under Contract No. DE-AC02-76SF00515. The AFM measurements were done by Andrey V. Malkovskiy and the XPS measurements by Chuck Hitzman at the Stanford Nano Shared Facilities (SNSF), supported by the National Science Foundation under Award No. ECCS-1542152. The scanning SQUID microscope and sensors used in this experiment were developed with support by an NSF IMR-MIP Grant No. DMR-0957616. C.A. was supported by an Air Force Office of Scientific Research Grant No. FA9550-09-1-0583. We would like to thank Vladimir Kogan for useful conversations.

S.I.D. and R.R.U. contributed equally to this work.

[1] J. G. Bednorz and K. A. Muller, Possible high T_c superconductivity in the BaLaCuO system, Z. Phys. B: Conden. Matter **64**, 189 (1986).

[2] C. C. Tsuei and J. R. Kirtley, Pairing symmetry in cuprate superconductors, Rev. Mod. Phys. **72**, 969 (2000).

[3] M. R. Norman and C. Pepin, The electronic nature of high temperature cuprate superconductors, Rep. Prog. Phys. **66**, 1547 (2003).

[4] P. A. Lee, From high temperature superconductivity to quantum spin liquid: Progress in strong correlation physics, Rep. Prog. Phys. **71**, 012501 (2008).

[5] L. Nie, G. Tarjus, and S. A. Kivelson, Quenched disorder and vestigial nematicity in the pseudogap regime of the cuprates, Proc. Natl. Acad. Sci. USA **111**, 7980 (2014).

[6] E. Berg, E. Fradkin, and S. A. Kivelson, Charge-4e superconductivity from pair-density-wave order in certain high-temperature superconductors, Nat. Phys. **5**, 830 (2009).

[7] M. Fujita, H. Goka, K. Yamada, and M. Matsuda, Competition Between Charge- and Spin-Density-Wave Order and Superconductivity in $La_{1.875}Ba_{0.125-x}Sr_xCuO_4$, Phys. Rev. Lett. **88**, 167008 (2002).

[8] J. R. Kirtley, Fundamental studies of superconductors using scanning magnetic imaging, Rep. Prog. Phys. **73**, 126501 (2010).

[9] J. R. Kirtley, B. Kalisky, J. A. Bert, C. Bell, M. Kim, Y. Hikita, H. Y. Hwang, J. H. Ngai, Y. Segal, F. J. Walker *et al.*, Scanning SQUID susceptometry of a paramagnetic superconductor, Phys. Rev. B **85**, 224518 (2012).

[10] J. R. Kirtley, M. B. Ketchen, K. G. Stawiasz, J. Z. Sun, W. J. Gallagher, S. H. Blanton, and S. J. Wind, High-resolution scanning SQUID microscope, Appl. Phys. Lett. **66**, 1138 (1995).

[11] B. W. Gardner, J. C. Wynn, P. G. Björnsson, E. W. J. Straver, K. A. Moler, J. R. Kirtley, and M. B. Ketchen, Scanning superconducting quantum interference device susceptometry, Rev. Sci. Instrum. **72**, 2361 (2001).

[12] J. R. Kirtley, L. Paulius, A. J. Rosenberg, J. C. Palmstrom, C. M. Holland, E. M. Spanton, D. Schiessl, C. L. Jermain, J. Gibbons, Y.-K.-K. Fung *et al.*, Scanning SQUID susceptometers with sub-micron spatial resolution, Rev. Sci. Instrum. **87**, 093702 (2016).

[13] J. H. Haeni, C. D. Theis, and D. G. Schlom, RHEED intensity oscillations for the stoichiometric growth of $SrTiO_3$ thin films by reactive molecular beam epitaxy, J. Electroceram. **4**, 385 (2000).

[14] A. Biswas, P. B. Rossen, J. Ravichandran, Y.-H. Chu, Y.-W. Lee, C.-H. Yang, R. Ramesh, and Y. H. Jeong, Selective a- or b-site single termination on surfaces of layered oxide $SrLaAlO_4$, Appl. Phys. Lett. **102**, 051603 (2013).

[15] F. Otto, Attocube scanning SQUID platform, Accessed January 28, 2018 from http://www.attocube.com/attomicroscopy/microscopy-solutions/squid.

[16] J. R. Kirtley, C. C. Tsuei, K. A. Moler, V. G. Kogan, J. R. Clem, and A. J. Turberfield, Variable sample temperature scanning superconducting quantum interference device microscope, Appl. Phys. Lett. **74**, 4011 (1999).

[17] See Supplemental Material at http://link.aps.org/supplemental/10.1103/PhysRevB.98.014506 for susceptibility touchdown data, fits, and differences between fits and data, for the five samples that showed diamagnetic shielding at 5 K.

[18] H. Sato, A. Tsukada, M. Naito, and A. Matsuda, Absence of 1/8 anomaly in strained thin films of $La_{2-x}Ba_xCuO_{4+\delta}$, Phys. Rev. B **62**, R799 (2000).

[19] M. Fujita, H. Goka, K. Yamada, J. M. Tranquada, and L. P. Regnault, Stripe order, depinning, and fluctuations in $La_{1.875}Ba_{0.125}Cuo_4$ and $La_{1.875}Ba_{0.075}Sr_{0.050}CuO_4$, Phys. Rev. B **70**, 104517 (2004).

[20] M. Hücker, M. v. Zimmermann, G. D. Gu, Z. J. Xu, J. S. Wen, G. Xu, H. J. Kang, A. Zheludev, and J. M. Tranquada, Stripe order in superconducting $La_{2-x}Ba_xCuO_4$ ($0.095 \leqslant x \leqslant 0.155$), Phys. Rev. B **83**, 104506 (2011).

[21] J. M. Tranquada, Exploring intertwined orders in cuprate superconductors, Phys. B **460**, 136 (2015).

[22] O. Daldini, P. Martinoli, J. L. Olsen, and G. Berner, Vortex-Line Pinning by Thickness Modulation of Superconducting Films, Phys. Rev. Lett. **32**, 218 (1974).

[23] P. Martinoli, Static and dynamic interaction of superconducting vortices with a periodic pinning potential, Phys. Rev. B **17**, 1175 (1978).

[24] J. Pons, IUCr martensitic phase transformations: the memory of shape, accessed March 15, 2018 from https://www.iucr.org/news/newsletter/volume-7/number-2/martensitic-transformations.

[25] J. P. Sethna, in *Entropy, Order Parameters, and Complexity* (Clarendon Press, Oxford, 2017), p. 250.

[26] W. Y. Liang, C. T. Lin, J. Chrosch, Y. Yan, and E. K. H. Salje, Tetragonal tweed phase superconducting YBCO single crystals, Adv. Supercond. VII **1**, 137 (1995).

[27] J.-P. Locquet, J. Perret, J. Fompeyrine, E. Mächler, J. W. Seo, and G. Van Tendeloo, Doubling the critical temperature of $La_{1.9}Sr_{0.1}CuO_4$ using epitaxial strain, Nature **394**, 453 (1998).

[28] G. Blatter, M. V. Feigel'man, V. B. Geshkenbein, A. I. Larkin, and V. M. Vinokur, Vortices in high-temperature superconductors, Rev. Mod. Phys. **66**, 1125 (1994).

[29] J. Pearl, Current distribution in superconducting films carrying quantized fluxoids, Appl. Phys. Lett. **5**, 65 (1964).

[30] G. Carneiro and E. H. Brandt, Vortex lines in films: Fields and interactions, Phys. Rev. B **61**, 6370 (2000).

[31] Y. Wang, S. D. Edkins, M. H. Hamidian, J. C. S. Davis, E. Fradkin, and S. A. Kivelson, Pair density waves in superconducting vortex halos, Phys. Rev. B **97**, 174510 (2018).

[32] O. M. Auslaender, L. Luan, E. W. J. Straver, J. E. Hoffman, N. C. Koshnick, E. Zeldov, D. A. Bonn, R. Liang, W. N. Hardy, and K. A. Moler, Mechanics of individual isolated vortices in a cuprate superconductor, Nat. Phys. **5**, 35 (2008).